Atmos. Chem. Phys. Discuss., doi:10.5194/acp-2016-1167, 2017
Manuscript under review for journal Atmos. Chem. Phys.
Published: 12 January 2017

Atmospheric Chemistry and Physics Discussions
Open Access

Abrupt seasonal transitions in land carbon uptake in 2015

Chao Yue[1], Philippe Ciais[1], Ana Bastos[1], Frederic Chevallier[1], Yi Yin[1], Christian Rödenbeck[2]

[1]Laboratoire des Sciences du Climat et de l'Environnement, CEA-CNRS-UVSQ, UMR8212, Gif-sur-Yvette, France

[2] Max Planck Institute for Biogeochemistry, Jena, Germany.

Corresponding author: Chao Yue, chao.yue@lsce.ipsl.fr

Abstract

The year 2015 saw a record atmospheric CO_2 growth rate associated with a weaker than usual land carbon sink. Paradoxically, it was also the greenest year since 2000 according to satellite observations of vegetation greenness. To reconcile these two seemingly paradoxical observations, we examined the patterns of CO_2 fluxes using two atmospheric inversions. Inversion results indicate that the year 2015 had a higher than usual northern land carbon uptake in spring and summer, consistent with the greening anomaly. This higher uptake was however followed by a larger source of CO_2 in autumn, suggesting a coupling between growing season uptake and late season release of CO_2. For the tropics and Southern Hemisphere, a strong and abrupt transition toward a large carbon source for the last trimester of 2015 is discovered, concomitant with the El Niño development. This abrupt transition of terrestrial tropical CO_2 fluxes between two consecutive seasons is the largest ever found in the inversion records.

1 Introduction

The first monitoring station for background atmospheric CO_2 concentration was established at Mauna Loa in 1958. The record since then shows that atmospheric CO_2 continued to rise in response to anthropogenic emissions. However, the atmospheric CO_2 growth rate (AGR) has been lower than that implied by anthropogenic emissions alone, because land ecosystems and the oceans have absorbed part of the emitted CO_2 (Canadell et al., 2007; Le Quéré et al., 2016).

Atmos. Chem. Phys. Discuss., doi:10.5194/acp-2016-1167, 2017
Manuscript under review for journal Atmos. Chem. Phys.
Published: 12 January 2017

Atmospheric Chemistry and Physics
Open Access
EGU
Discussions

Although on multi-decadal time scale, carbon uptake by land and ocean has kept in pace with growing carbon emissions (Ballantyne et al., 2012; Li et al., 2016), large year-to-year fluctuations occur in the terrestrial carbon sink, mainly in response to climate variations induced by El Niño–Southern Oscillation (ENSO) (Wang et al., 2013, 2014) and other occasional events such as volcanic eruptions (Gu et al., 2003).

In 2015, the global monthly atmospheric CO_2 concentration surpassed 400 p.p.m. for the first time since the start of the measurements, with an unprecedented large annual growth rate of 2.96±0.09 p.p.m. yr^{-1} (https://www.esrl.noaa.gov/gmd/ccgg/trends/global.html#global_growth). This record-breaking AGR occurred simultaneously with a high value of the ENSO index (Betts et al., 2016) and the warmest land temperature on record since 1880 (https://www.ncdc.noaa.gov/cag/time-series/global/globe/land/ytd/12/1880-2015). But at the same time, 2015 was also shown to have the greenest growing season of the Northern Hemisphere since 2000 (Bastos et al., 2016). Widespread abnormally high positive anomalies of the normalized difference vegetation index (NDVI) were observed from the Terra satellite's Moderate-resolution imaging spectroradiometer (MODIS) sensor, in particular over eastern North America and large parts of Siberia. On the one hand, strong greening is expected to enhance northern land carbon uptake during the growing season; on the other hand the strong El Niño event in the second half of 2015 increased fire emissions in tropical Asia (Huijnen et al., 2016; Yin et al., 2016) and likely caused a loss of plant biomass and reduced carbon uptake, possibly associated with the prevailing high temperatures and reduced rainfall (Ahlström et al., 2015; Jiménez-Muñoz et al., 2016).

To reconcile the observed maximum global land greening with the record-high AGR in 2015, we examined land-atmosphere carbon fluxes estimated from two atmospheric inversions encompassing the last three decades and assimilating atmospheric CO_2 mole fraction records from a large number of *in situ* and flask records: the Copernicus Atmosphere Monitoring Service inversion (CAMS, version r15v3) (Chevallier et al., 2005, 2010) and the Jena CarboScope atmospheric inversion (version s04_v3.8, hereafter abbreviated as Jena04, update from Rödenbeck, 2005; Rödenbeck et al., 2003). We focus on seasonal patterns in the land carbon uptake during 2015, relative to the long-term trend of 1981-2015. We then investigate how land

Atmos. Chem. Phys. Discuss., doi:10.5194/acp-2016-1167, 2017
Manuscript under review for journal Atmos. Chem. Phys.
Published: 12 January 2017

ecosystems responded to the joint occurrences of record-breaking warming, extreme greening, and the end-of-year El Niño event, to understand how land ecosystems contributed to the high AGR in 2015.

2 Data and methods

2.1 Data sets

2.1.1 Atmospheric inversion data

We used two gridded land and ocean carbon uptake data sets based on atmospheric CO_2 observations, namely the Copernicus Atmosphere Monitoring Service (CAMS) inversion system developed at LSCE (Chevallier et al., 2005, 2010) and the Jena CarboScope inversion system developed at the MPI for Biogeochemistry Jena (update of Rödenbeck, 2005; Rödenbeck et al., 2003). Atmospheric inversions use atmospheric CO_2 concentration at observation sites, combined with an atmospheric transport model as well as prior information on carbon emissions from fossil fuel burning and on carbon exchange between the atmosphere and land (and ocean), to estimate land- and ocean-atmosphere net carbon fluxes that minimize a Bayesian cost function, which measures the mismatch between observed and simulated atmospheric CO_2 mixing ratios. Detailed information inversions could be found in respective sources as mentioned above.

The CAMS inversion data (version r15v3) were provided for 1979-2015 with a weekly time-step and a spatial resolution of 1.875° latitude and 3.75° longitude. The Jena CarboScope inversion provides daily fluxes at a spatial resolution of 3.75° latitude and 5° longitude. It offers a series of runs that use differently large station sets with complete data coverage over time, in order to avoid spurious flux variations from a changing station network. From these runs, we used s04_v3.8 (shortened as Jena04 in the main text and supplementary material) includes the largest number of measurement sites, to allow more robust constraining of carbon exchanges in 2015 (see http://www.bgc-jena.mpg.de/CarboScope/ for more details on other configurations). The s04_v3.8 run has a validity period as 2004–2015, although it does provide the data for the whole time span of 1981–2015. In the calculation of the long-term linear trend, we exceptionally use this run outside its period of validity; from a comparison of the linear trends over the latitudinal regions examined in this study between the s04_v3.8 and the long s81_v3.8 runs we established that this was possible in this case.

Atmos. Chem. Phys. Discuss., doi:10.5194/acp-2016-1167, 2017
Manuscript under review for journal Atmos. Chem. Phys.
Published: 12 January 2017

Atmospheric Chemistry and Physics Discussions

2.2.2 Atmospheric CO_2 growth rates, NDVI and climate data

Atmospheric CO_2 growth rates were retrieved from the Global Monitoring Division, Earth System Research Laboratory (ESRL), NOAA (http://www.esrl.noaa.gov/gmd/ccgg/trends/global.html). We used NDVI data between 2000 and 2015 from MODIS Terra Collection 6, re-gridded at 0.5° resolution and monthly time-step. The NDVI anomalies are calculated at pixel level as the standardized monthly NDVI (i.e., de-seasonalized) relative to the reference period of 2000–2014. Climate fields are from ERA interim reanalysis (Dee et al., 2011) at 0.5° resolution and monthly time-step. We used air temperature, precipitation and volumetric soil water content (%) integrated over the soil column to a depth of 2.89 m.

2.1.3 Indices for El Niño–Southern Oscillation (ENSO) states and fire emission data

We examined the seasonal variations of the carbon cycle in 2015 in relation to ENSO events and compared the year 2015 with the 1997–1998 El Niño event. The Multivariate ENSO Index (MEI, http://www.esrl.noaa.gov/psd/enso/mei/) was used to indicate the ENSO state. MEI is a composite index calculated as the first unrotated principal component of six ENSO-relevant variables for each of the twelve sliding bi-monthly seasons. The 12 bi-monthly MEI values of each year are summed to obtain the annual MEI. To examine the potential role of fire emissions in the land carbon balance in 2015, we used the GFED4s carbon emission data at daily time-step and 0.25° spatial resolution (http://www.globalfiredata.org/data.html). Monthly fire-carbon emissions were calculated for the regions and were examined for 1997–2015.

2.2 Data analysis

2.2.1 NDVI rank analysis and greening trend

First, we calculated seasonal mean standardized NDVI for each pixel and each year of the period 2000–2015. We examined four seasons: Q1 (January–March), Q2 (April–June), Q3 (July–September) and Q4 (October–December). Given a season and a pixel, the annual time series of seasonal NDVI for 2000-2015 were ranked in ascending order so that each year could be labelled by a rank, with 1 being the lowest and 16 the highest rank. A spatial map of NDVI rank was then obtained for each year for the given season. Vegetated area fraction with the highest rank for different years was obtained, with the sum of these fractions yielding unity. This procedure was repeated for all four seasons to generate four seasonal time series, with each containing the vegetation land fractions with highest NDVI for different years. Finally, a composite map was made for year 2015, by merging pixels with the highest rank of all four seasons in 2015.

2.2.2 Analysis of 2015 land carbon uptake dynamics

Annual land and ocean carbon uptakes and carbon emissions from the two inversions were calculated for the globe over their period of overlap, 1981–2015. AGRs from NOAA/ESRL over 1981–2015 were converted into Pg C using a conversion factor of 2.12 Pg C p.p.m.$^{-1}$ (Ballantyne et al., 2012; Le Quéré et al., 2016), assuming that all the atmosphere is well mixed within one year. For comparison, land and ocean net carbon uptakes for 1981–2015 were retrieved from the Global Carbon Project (Le Quéré et al., 2016). For this purpose, a carbon flux of 0.45 Pg C yr^{-1} is subtracted from the inversion-derived land carbon uptakes and is added to ocean carbon uptakes to account for the pre-industrial land-to-ocean carbon fluxes (Jacobson et al., 2007), following Le Quéré et al. (2016).

The record high AGR in 2015 was a composite collectively determined by carbon emissions from fossil fuel burning and industry, and land and ocean carbon uptakes, all being impacted by a historical trend. Thus to properly attribute the 2015 AGR to historical trend and interannual variation, annual time series of carbon emissions, land and ocean carbon uptakes, and AGRs from NOAA/ESRL over 1981-2015 were linearly detrended to generate the detrended anomalies of AGR, emissions, and land and ocean carbon uptakes. The percentages of anomalies in carbon emissions, land and ocean sink in 2015 to the 2015 AGR anomaly were then calculated as relative contributions by each factor to the 2015 AGR anomaly.

Seasonal land carbon uptakes were also calculated (the 0.45 Pg C yr^{-1} correction was not applied). We then examined the seasonal anomalies of 2015 land carbon uptake over different regions and the globe, and the seasonal transitions. The same linear detrending was done for 1981-2015. The globe was divided into two latitude bands: Boreal and temperate Northern Hemisphere (BoTeNH, latitude > 23.5°N) and tropics and extratropical Southern Hemisphere (TroSH, latitude < 23.5°N). The BoTeNH is further divided into boreal Northern Hemisphere (BoNH, latitude > 45°N) and

Atmos. Chem. Phys. Discuss., doi:10.5194/acp-2016-1167, 2017
Manuscript under review for journal Atmos. Chem. Phys.
Published: 12 January 2017

temperate Northern Hemisphere (TeNH, 23.5° < latitude < 45°N) for further discussion. Seasonal land carbon uptake transitions are calculated as the land sink anomaly in a given season minus that of the former one. When examining transitions of land carbon uptake anomalies by the CAMS inversion, we found the year 1993 has an extreme small Q3→Q4 global transition (-2.85 Pg C within 6 months, < -4σ, the second lowest being the year 2015 with -1.0 Pg C) albeit with a reasonable annual land carbon uptake (3.75 Pg C yr^{-1}). This is linked with an extreme high Q3 and low Q4 uptake in this year, which could not be explained by any known carbon cycle mechanisms. This is thus identified as a result of numerical instability of the inversion system and consequently the year 1993 has been removed from all the seasonal analyses. Finally, seasonal linear detrending was also performed at grid-cell level for land carbon uptakes for both inversions, as well as air temperature, precipitation and soil water content.

3 Results

3.1 Vegetation greening in 2015

Figure 1a illustrates where and when higher-than-normal greenness conditions were observed in different seasons of the year 2015, compared to other years of 2000–2015 (see Supplementary Fig. 1 for greenness distribution for each season). On average 17% of vegetated land shows record seasonal NDVI in 2015. The year with the second highest NDVI is 2014 having only 11% vegetated area with record NDVI. An increase of the record-breaking NDVI occurrence over time was clearly demonstrated (Fig. 1b). In short, 2015 clearly stands out as a greening outlier, having the highest proportion of vegetated land being the greenest for all four seasons except for the first season (despite the fact that for Q1, 2015 is still the second highest, Q1 = January to March).

For Northern Hemisphere boreal and temperate regions, the seasons with highest NDVI in 2015 are Q2 and Q3 (Q2 = April to June; Q3 = July to September), corresponding to the growing season from spring to early autumn. A pronounced greening anomaly in Q2 occurred in western to central Siberia, western Canada and Alaska and eastern and southern Asia (Supplementary Fig. 1). Central and eastern Siberia and eastern North America showed marked greening in Q3. Strong and widespread greening also occurred in the tropics during Q3 over Amazonia and the savanna (or cerrado) of eastern South America, but this positive greening disappeared in Q4 (Q4

Atmos. Chem. Phys. Discuss., doi:10.5194/acp-2016-1167, 2017
Manuscript under review for journal Atmos. Chem. Phys.
Published: 12 January 2017

Atmospheric Chemistry and Physics
Discussions

= October to December) especially over central to eastern Amazonia with the development of El Niño (Supplementary Fig. 1).

3.2 Global carbon balance for 1981-2015

Figure 2 shows the time series of fossil and industry carbon emissions, NOAA/ESRL AGR rates linked with ENSO climate oscillations as indicated by the Multivariate ENSO Index (MEI), and land and ocean carbon sinks for the common period of the two inversions (1981–2015) and the estimates by the Global Carbon Project (GCP). Emissions show a clear increase with time, however AGRs are more varying. The record high AGR of 2.96 p.p.m. in 2015 exceeds those in all other previous years including the extreme El Niño event in 1997–98. Interannual variability in AGR is mainly caused by land carbon sink fluctuations, with Pearson's correlation coefficients between detrended AGR and land sink < -0.8 ($p<0.01$) for both inversions (Pearson's correlation coefficient between detrended AGR and MEI being 0.27, $p<0.1$). The root mean square differences between inversion and GCP carbon sinks are 0.70 and 0.65 Pg C yr^{-1} for CAMS and Jena04 respectively for the land, and ~0.5 PgC yr^{-1} for the ocean for bother inversions, within the uncertainties of 0.8 and 0.5 Pg C yr^{-1} over 1981–2015, respectively for land and ocean as reported by GCP. The interannual variability of detrended sink anomalies for the land agrees well between inversions and GCP (with Pearson's correlation coefficient being 0.9 for both inversions, $p < 0.01$).

For 2015, the prescribed carbon emissions in the CAMS inversion are 9.9 Pg C yr^{-1}, of which 2.0 Pg C are absorbed by ocean, 1.7 Pg C by land ecosystems, with 6.2 Pg C remaining in the atmosphere, which matches the AGR from background stations of 6.3 Pg C assuming a conversion factor of 2.12 Pg C $p.p.m.^{-1}$ (Ballantyne et al., 2012; Le Quéré et al., 2016) and considering a measurement uncertainty of AGR as 0.09 p.p.m. (0.2 Pg C) for 2015. When land carbon fluxes from the inversion are linearly detrended over 1981-2015, the terrestrial sink in 2015 is 1.2 Pg C lower than normal (i.e., the trend value), but this is not an extreme value — it is only the seventh weakest sink since 1981. This weaker land uptake accounts for 82% of the positive AGR anomaly, which is 1.45 Pg C in 2015 by subtracting a linear temporal trend. Jena04 yields an AGR in 2015 that is 0.13 p.p.m. lower than the AGR based on background stations only, a difference close to the observation uncertainty. After removing the linear trends over time similarly as for CAMS inversion, the land carbon uptake anomaly is -0.3 Pg C yr^{-1} in 2015 by Jena04 data, or 20% of the observed AGR anomaly, the remaining being explained by positive anomaly in fossil fuel emissions (34%), negative anomaly in ocean sink (20%), and the difference between modelled AGR and NOAA/ESRL reported AGR. Note that the land sink by GCP for 2015 is much lower than the two inversions, with detrended anomaly lower than that of CAMS, indicating even larger contribution from land to the high anomaly of AGR.

3.3 Seasonal land carbon uptake dynamics in 2015

To explain the seemingly paradox in 2015 between high greening and an only moderate terrestrial uptake, we examined seasonal land carbon flux dynamics using both inversions. The land carbon flux anomalies for each season and different regions of the globe are calculated (linearly detrended over 1981-2015), and shown in Fig. 3 (refer to Supplementary Fig. 2 for spatial distribution of flux anomalies). Positive anomalies indicate enhanced sink (or reduced source) against the linear trend (i.e., the normal state), while negative ones indicate the reverse.

At seasonal scale, both inversions indicate positive carbon uptake anomalies during Q2 and Q3 for boreal and temperate Northern Hemisphere (BoTeNH, latitude > 23.5°N), consistent with marked greening in central to eastern Siberia, eastern Europe and Canada (Fig. 1) as outlined above. However, an extreme follow-up negative (source) anomaly occurred in Q4 (Fig. 3b). These negative anomalies were lower than the 10th percentile of all anomalies in Q4 over time for both inversions and they partly cancelled the extra uptake in Q2 and Q3. As a result, on the annual time scale, the CAMS inversion shows an almost neutral land flux anomaly in BoTeNH, while the Jena04 inversion still indicates a significant positive annual anomaly.

For the tropics and extratropical Southern Hemisphere (TroSH, latitude < 23.5°N), both inversions show a weak negative land carbon anomaly for Q1 (mean value of -0.10 Pg C) in 2015, moderate anomalies in Q2 (of differing signs, with a negative one of -0.3 Pg C in CAMS and a positive one of 0.2 Pg C in Jena04). Q3 anomalies are almost carbon neutral for both inversions. In stark contrast, between Q3 and Q4, both inversions show an abrupt shift toward an abnormally big land carbon source (i.e., negative anomalies of ~ -0.7 Pg C against a carbon source expected from the linear trend, lower than 10th percentile over time in both inversions).

Atmos. Chem. Phys. Discuss., doi:10.5194/acp-2016-1167, 2017
Manuscript under review for journal Atmos. Chem. Phys.
Published: 12 January 2017

On the annual time scale, CAMS shows a large negative anomaly of -1.2 Pg C. For Jena04, sink and source effects in Q1–Q3 cancelled each other, leaving the annual anomaly the same as in Q4.

Over the globe, the Jena04 inversion shows an abnormally strong sink during Q2 (normal state being a net carbon sink), owing to synergy of enhanced Q2 uptakes in both BoTeNH and TroSH. This abnormally enhanced uptake partly counteracted the strong shift toward source in Q4 (normal state being a net carbon source), leaving a small negative annual land carbon balance of -0.3 Pg C. For the CAMS inversion, because of the co-occurrence of enhanced carbon release in BoTeNH and the sudden shift toward a large carbon source in TroSH both in Q4 (normal states being both net carbon sources), the land shows a strong global shift toward being a source in Q4, leaving a negative annual carbon anomaly of -1.2 Pg C (i.e., carbon sink being reduced compared with the normal state).

These consistent results from both inversions point to very strong seasonal shifts in the land carbon balance as an emerging feature of 2015. We thus calculated ***transitions*** in land carbon uptake anomaly as the first-order difference in flux anomalies between two consecutive seasons (defined as the anomaly in a given season minus that in the former one) for all years of the period 1982-2015 (Fig. 4). The ranks of transitions for different seasons relative to other years between the two inversions are broadly similar, except for Q1→Q2 and Q2→Q3 in TroSH, mainly due to the differences between the two inversions in seasonal land-carbon uptake anomaly in Q2 (Fig. 3b). On the global scale, both inversions show an extreme transition to a negative uptake anomaly for Q3→Q4, with 2015 being the largest transition of the period 1982-2015 (a transition towards an enhanced carbon source of -1.0 Pg C in 6 months). The abnormal transitions for Q3→Q4 on the global scale are located in the TroSH region, where both inversions show that during 1982-2015 the largest transition occurred in 2015. For BoTeNH, both inversions showed strong transitions toward positive anomaly for Q1→Q2; however, the same strong transition toward source anomaly occurred in Q3→Q4, partly cancelling the sink effects during growing seasons.

4 Discussion

4.1 Seasonal land carbon uptake transitions in northern latitudes

The two inversions consistently allocate a strong positive carbon uptake anomaly in the BoTeNH during spring, which persists through summer (Q2–Q3): an extreme sink anomaly is simulated in Q2 by Jena04, but a more moderate one by CAMS (still above the 75th percentile). The strong sink in Q2 simulated by CAMS is dominated by temperate Northern Hemisphere regions (TeNH, 23.5° < latitude < 45°N, Supplementary Fig. 3). For Q3, an extreme carbon sink anomaly occurs in boreal Northern Hemisphere (BoNH, latitude > 45°N) in CAMS; however, an equally strong negative anomaly (i.e., reduced sink) was found in TeNH in the same season, leaving the whole boreal and temperate Northern Hemisphere (BoTeNH) only a moderate enhanced sink anomaly. Thus for TeNH alone, CAMS indicates extreme seasonal shift from a positive anomaly in Q2 to a negative one in Q3, implying abrupt seasonal transitions probably resulting from enhanced ecosystem CO_2 release after growing-season uptake.

Jena04 inversion agrees with a higher-than-normal sink in TeNH (23.5° < latitude < 45°N) during spring (Q2). It also reports a moderate positive anomaly for Q3 in BoNH, but does not show a strong negative anomaly (i.e., reduced sink) in TeNH in Q3 as CAMS does. This is possibly related to differences in the measurement station data used, to different land prior fluxes (from the ORCHIDEE model in CAMS, and the LPJ model in Jena CarboScope), or to the fact that Jena inversion has a larger a-priori spatial error correlation length scale for its land fluxes (1275 km) than CAMS (500 km) (Chevallier et al., 2010; Rödenbeck et al., 2003). Nonetheless, both inversions consistently indicate that the enhancement of CO_2 uptake during spring and summer at the northern hemispheric scale was subsequently offset by an extreme source anomaly in autumn (Q4).

The transition from carbon sink anomalies during Q2 and Q3 in the Northern Hemisphere to a source anomaly during Q4 could be related with prevailing high temperatures in Q4, especially over most of northern America, and central to eastern Siberia and Europe (Supplementary Fig. 4a). The strong source anomaly in temperate regions during summer (Q3) as indicated by CAMS may also be partly due to the extreme drought that affected Europe (Supplementary Fig. 4b, see also Orth et al., 2016) and led to vegetation browning (decreased NDVI) in this region (Bastos et al., 2016). The transition toward carbon source in Q4, albeit strong uptake and high greening during the preceding seasons (especially in southern to eastern Asia in Q4), highlights the

Atmos. Chem. Phys. Discuss., doi:10.5194/acp-2016-1167, 2017
Manuscript under review for journal Atmos. Chem. Phys.
Published: 12 January 2017

Atmospheric Chemistry and Physics Discussions

importance of carbon release in the autumn (Piao et al., 2008) and the carry-over effect of higher leaf and fine root biomass produced in spring and summer being decomposed a few months later at the end of the year.

4.2 Seasonal land carbon uptake transitions in tropics and influences of El Niño and vegetation fire

The abrupt transition to abnormal source in the tropics and extratropical Southern Hemisphere was paralleled by a marked decrease in precipitation and an increase in temperature in Q4, with the development of El Niño in Q2–Q3 (Supplementary Fig. 5). Here El Niño development is indicated by the rise of the MEI. This abrupt transition is consistent with the expected response of tropical and sub-tropical southern ecosystems during previous El Niño events (Ahlström et al., 2015; Cox et al., 2013; Poulter et al., 2014; Wang et al., 2013, 2014).

Compared with the 1997–98 El Niño, which was of similarly extreme magnitude, the 2015 El Niño started much earlier with positive MEI appearing during the first half of 2014. Since then until Q3 and Q4 in 2015 when El Niño began to reach its peak, the tropics and Southern Hemisphere saw continuous higher-than-normal temperatures, with continually decreasing precipitation and accumulating deficit in soil water content (Supplementary Fig. 5). From Q3 to Q4, a steep decline is further observed in both precipitation and soil moisture with stagnating high temperature anomaly, which is probably a major cause of the abrupt shift toward carbon source anomaly. The CAMS inversion shows a carbon source anomaly in Q4 of 2015 slightly smaller than that in Q3 of 1997, while the Jena04 inversions shows almost equal magnitudes of loss in land sink strength between these two extreme El Niño events. On the one hand, El Niño in late 2015 started with an early onset and built upon the cumulative effects of the drought since the beginning of the year; it thus came with larger negative anomaly in precipitation and soil water content than the 1997–98 El Niño. This sequence of events might favour a stronger land carbon source. On the other hand, the fire emission anomaly in the tropics in 2015 was less than half of that in 1997 at the peak of El Niño (Fig. S5), which might contribute to a smaller land source anomaly in 2015 than in 1997–98.

El Niño events are usually associated with increased vegetation fires, and these have a large

Atmos. Chem. Phys. Discuss., doi:10.5194/acp-2016-1167, 2017
Manuscript under review for journal Atmos. Chem. Phys.
Published: 12 January 2017

Atmospheric Chemistry and Physics Discussions

impact on the global carbon cycle (van der Werf et al., 2004). Global fire emissions of carbon reached 3.0 and 2.9 Pg C in 1997 and 1998 according to the GFED4s data. These two years produced the largest source of fire-emitted carbon for the entire period 1997–2015. Global fire emissions in 2015 reached 2.3 Pg C, close to the 1997-2015 average (2.2 Pg C yr^{-1}) but 23–24% lower than 1997–98 — the difference mainly occurring in the southern tropics (0–23.5°S, Fig. S5). In particular, carbon emissions from deforestation and peat fires were two times lower in 2015 (0.6 Pg C) compared with 1997 (1.2 Pg C) (GFED4s data), and emissions for these types of fires are more likely to be a net source contribution, because they cannot be compensated by vegetation regrowth within a short time. Fire emission data thus suggest a smaller contribution from fires to AGR in 2015 than 1997–98. If both annual time series of AGR and global fire-carbon emissions are detrended within their overlapping period of 1997-2015, fire-carbon emissions have an anomaly of 0.4 Pg C yr^{-1} in 2015, explaining only 29% of the AGR anomaly.

4.3 Data uncertainties and perspective

On the global and hemispheric scales, the inversion-derived land- and ocean-atmosphere fluxes are well constrained by the observed atmospheric CO_2 growth rates on measurement sites. However, because the observational network is heterogeneous and sites are sparsely distributed (Supplementary Fig. 6), land CO_2 fluxes cannot be resolved precisely over each grid cell (Kaminski et al., 2001) and some regions are better constrained than others. This could hinder the precise matching between gridded CO_2 flux maps and climate states or the occurrence of climate extremes; consequently, exact attribution of carbon uptake transitions into different climate drivers could be elusive. Further, a few other uncertainties matter for the specific objective of this study. First, the atmospheric network increased over time, so that the inversions have a better ability to detect and quantify a sharp transition in CO_2 fluxes occurring in the last than in the first decade of the period analysed. This might hide the detection of other more extreme end-of-year carbon transitions during early years of our target period (1981-2015). Second, because measurements for the early 2016 are not used in the CAMS inversion and not completely available in the Jena inversion, the constraining of last season in 2015 is weaker than for the other three seasons. This could partly influence the exact magnitude of the extreme Q4 negative anomaly in land carbon uptake reported here. Third, the sparse sites located in the boreal Eurasia and tropical regions might diminish the ability of inversion systems to robustly allocation carbon fluxes spatially, which could yield high uncertainty in the carbon fluxes diagnosed for these regions (van der Laan-Luijkx et al., 2015; Stephens et al., 2007).

Despite these uncertainties, the abrupt transition of CO_2 fluxes analysed here is the largest ever found in the inversion records. While transition to a strong source in TroSH is congruent with the expected response of ecosystems to the peak of an El Niño event, it is not completely clear which mechanisms are driving the reported abrupt seasonal transitions on the global scale. For instance, for the tropics and Southern Hemisphere, it is unclear whether the dry conditions already in place before the full development of El Niño implied moderate Q2 and Q3 vegetation carbon uptakes followed by moderate respiration as well in Q4, or if it is mainly due to enhanced respiration in late 2015 that dominated such a transition. For the boreal and temperate Northern Hemisphere, further investigation is still needed to verify whether a coupling between strong spring/summer uptake and autumn release is something intrinsic to natural ecosystems, or if strong transitions to autumn release are triggered by abrupt climate shifts. This could be evaluated by process-based and data-driven models to partition the overall sink anomaly into individual responses of photosynthesis and respiration, but that is beyond the scope of this work. Our results point to the need to better understand the drivers of carbon dynamics at seasonal, or even shorter time scales at the regional to global level, especially the link between such dynamics and climate extremes. Such understanding would help better predictions of the response of the carbon cycle to multiple long-term drivers such as atmospheric CO_2 growth and climate change.

5 Conclusions

We investigated seasonal dynamics of land carbon uptake in 2015 using data from two atmospheric inversions, focusing on reconciling the seemingly paradox between the greatest vegetation greenness and the highest atmospheric CO_2 growth rate. We found that lands in Northern Hemisphere started with a higher-than-normal sink for the northern growing seasons, consistent with enhanced vegetation greenness partly owing to elevated warming, however this enhanced sink was partly balanced by enhanced carbon release in autumn and winter. For tropics and Southern Hemisphere, a strong and abrupt transition toward a large carbon source for the last quarter of 2015 was found, concomitant with the peak of El Niño development. This abrupt transition of terrestrial CO2 fluxes in the last quarter is the largest in the inversion records since

Atmos. Chem. Phys. Discuss., doi:10.5194/acp-2016-1167, 2017
Manuscript under review for journal Atmos. Chem. Phys.
Published: 12 January 2017

1981. The abrupt transitions in CO_2 fluxes diagnosed in this study form an interesting test bed for evaluating ecosystem models and gaining understanding of their controlling processes.

Atmos. Chem. Phys. Discuss., doi:10.5194/acp-2016-1167, 2017
Manuscript under review for journal Atmos. Chem. Phys.
Published: 12 January 2017

Atmospheric Chemistry and Physics
Discussions
Open Access

References

Ahlström, A., Raupach, M. R., Schurgers, G., Smith, B., Arneth, A., Jung, M., Reichstein, M., Canadell, J. G., Friedlingstein, P., Jain, A. K., Kato, E., Poulter, B., Sitch, S., Stocker, B. D., Viovy, N., Wang, Y. P., Wiltshire, A., Zaehle, S. and Zeng, N.: The dominant role of semi-arid ecosystems in the trend and variability of the land CO2 sink, Science, 348(6237), 895–899, doi:10.1126/science.aaa1668, 2015.

Ballantyne, A. P., Alden, C. B., Miller, J. B., Tans, P. P. and White, J. W. C.: Increase in observed net carbon dioxide uptake by land and oceans during the past 50 years, Nature, 488(7409), 70–72, doi:10.1038/nature11299, 2012.

Bastos, A.m Ciais, P., Park, T., Zscheischler, J., Yue, C., Barichivich, J., Myneni, R.B., Peng, S.S., Piao, S.L., Zhu Z. Was the extreme Northern Hemisphere greening in 2015 predictable? Submitted to Environ. Res. Lett.

Canadell, J. G., Le Quéré, C., Raupach, M. R., Field, C. B., Buitenhuis, E. T., Ciais, P., Conway, T. J., Gillett, N. P., Houghton, R. A. and Marland, G.: Contributions to accelerating atmospheric CO2 growth from economic activity, carbon intensity, and efficiency of natural sinks, Proc. Natl. Acad. Sci., 104(47), 18866–18870, 2007.

Chevallier, F., Fisher, M., Peylin, P., Serrar, S., Bousquet, P., Bréon, F.-M., Chédin, A. and Ciais, P.: Inferring CO2 sources and sinks from satellite observations: Method and application to TOVS data, J. Geophys. Res. Atmospheres, 110(D24), D24309, doi:10.1029/2005JD006390, 2005.

Chevallier, F., Ciais, P., Conway, T. J., Aalto, T., Anderson, B. E., Bousquet, P., Brunke, E. G., Ciattaglia, L., Esaki, Y., Fröhlich, M., Gomez, A., Gomez-Pelaez, A. J., Haszpra, L., Krummel, P. B., Langenfelds, R. L., Leuenberger, M., Machida, T., Maignan, F., Matsueda, H., Morguí, J. A., Mukai, H., Nakazawa, T., Peylin, P., Ramonet, M., Rivier, L., Sawa, Y., Schmidt, M., Steele, L. P., Vay, S. A., Vermeulen, A. T., Wofsy, S. and Worthy, D.: CO2 surface fluxes at grid point scale estimated from a global 21 year reanalysis of atmospheric measurements, J. Geophys. Res. Atmospheres, 115(D21), D21307, doi:10.1029/2010JD013887, 2010.

Cox, P. M., Pearson, D., Booth, B. B., Friedlingstein, P., Huntingford, C., Jones, C. D. and Luke, C. M.: Sensitivity of tropical carbon to climate change constrained by carbon dioxide variability, Nature, 494(7437), 341–344, doi:10.1038/nature11882, 2013.

Dee, D. P., Uppala, S. M., Simmons, A. J., Berrisford, P., Poli, P., Kobayashi, S., Andrae, U., Balmaseda, M. A., Balsamo, G., Bauer, P., Bechtold, P., Beljaars, A. C. M., van de Berg, L., Bidlot, J., Bormann, N., Delsol, C., Dragani, R., Fuentes, M., Geer, A. J., Haimberger, L., Healy, S. B., Hersbach, H., Hólm, E. V., Isaksen, L., Kållberg, P., Köhler, M., Matricardi, M., McNally, A. P., Monge-Sanz, B. M., Morcrette, J.-J., Park, B.-K., Peubey, C., de Rosnay, P., Tavolato, C., Thépaut, J.-N. and Vitart, F.: The ERA-Interim reanalysis: configuration and performance of the data assimilation system, Q. J. R. Meteorol. Soc., 137(656), 553–597, doi:10.1002/qj.828, 2011.

Gu, L., Baldocchi, D. D., Wofsy, S. C., Munger, J. W., Michalsky, J. J., Urbanski, S. P. and Boden, T. A.: Response of a Deciduous Forest to the Mount Pinatubo Eruption: Enhanced Photosynthesis, Science, 299(5615), 2035–2038, doi:10.1126/science.1078366, 2003.

Huijnen, V., Wooster, M. J., Kaiser, J. W., Gaveau, D. L. A., Flemming, J., Parrington, M., Inness, A., Murdiyarso, D., Main, B. and Weele, M. van: Fire carbon emissions over maritime southeast Asia in 2015 largest since 1997, Sci. Rep., 6, 26886, doi:10.1038/srep26886, 2016.

Atmos. Chem. Phys. Discuss., doi:10.5194/acp-2016-1167, 2017
Manuscript under review for journal Atmos. Chem. Phys.
Published: 12 January 2017

Atmospheric Chemistry and Physics Discussions

Jacobson, A. R., Mikaloff Fletcher, S. E., Gruber, N., Sarmiento, J. L. and Gloor, M.: A joint atmosphere-ocean inversion for surface fluxes of carbon dioxide: 1. Methods and global-scale fluxes, Glob. Biogeochem. Cycles, 21(1), GB1019, doi:10.1029/2005GB002556, 2007.

Jiménez-Muñoz, J. C., Mattar, C., Barichivich, J., Santamaría-Artigas, A., Takahashi, K., Malhi, Y., Sobrino, J. A. and Schrier, G. van der: Record-breaking warming and extreme drought in the Amazon rainforest during the course of El Niño 2015–2016, Sci. Rep., 6, 33130, doi:10.1038/srep33130, 2016.

Kaminski, T., Rayner, P. J., Heimann, M. and Enting, I. G.: On aggregation errors in atmospheric transport inversions, J. Geophys. Res. Atmospheres, 106(D5), 4703–4715, doi:10.1029/2000JD900581, 2001.

van der Laan-Luijkx, I. T., van der Velde, I. R., Krol, M. C., Gatti, L. V., Domingues, L. G., Correia, C. S. C., Miller, J. B., Gloor, M., van Leeuwen, T. T., Kaiser, J. W., Wiedinmyer, C., Basu, S., Clerbaux, C. and Peters, W.: Response of the Amazon carbon balance to the 2010 drought derived with CarbonTracker South America, Glob. Biogeochem. Cycles, 29(7), 2014GB005082, doi:10.1002/2014GB005082, 2015.

Li, W., Ciais, P., Wang, Y., Peng, S., Broquet, G., Ballantyne, A. P., Canadell, J. G., Cooper, L., Friedlingstein, P., Le Quéré, C., Myneni, R. B., Peters, G. P., Piao, S. and Pongratz, J.: Reducing uncertainties in decadal variability of the global carbon budget with multiple datasets, Proc. Natl. Acad. Sci., 113(46), 13104–13108, doi:10.1073/pnas.1603956113, 2016.

Orth, R., Zscheischler, J. and Seneviratne, S. I.: Record dry summer in 2015 challenges precipitation projections in Central Europe, Sci. Rep., 6, 28334, doi:10.1038/srep28334, 2016.

Piao, S., Ciais, P., Friedlingstein, P., Peylin, P., Reichstein, M., Luyssaert, S., Margolis, H., Fang, J., Barr, A., Chen, A., Grelle, A., Hollinger, D. Y., Laurila, T., Lindroth, A., Richardson, A. D. and Vesala, T.: Net carbon dioxide losses of northern ecosystems in response to autumn warming, Nature, 451(7174), 49–52, doi:10.1038/nature06444, 2008.

Poulter, B., Frank, D., Ciais, P., Myneni, R. B., Andela, N., Bi, J., Broquet, G., Canadell, J. G., Chevallier, F., Liu, Y. Y., Running, S. W., Sitch, S. and van der Werf, G. R.: Contribution of semi-arid ecosystems to interannual variability of the global carbon cycle, Nature, 509(7502), 600–603, doi:10.1038/nature13376, 2014.

Le Quéré, C., Andrew, R. M., Canadell, J. G., Sitch, S., Korsbakken, J. I., Peters, G. P., Manning, A. C., Boden, T. A., Tans, P. P., Houghton, R. A., Keeling, R. F., Alin, S., Andrews, O. D., Anthoni, P., Barbero, L., Bopp, L., Chevallier, F., Chini, L. P., Ciais, P., Currie, K., Delire, C., Doney, S. C., Friedlingstein, P., Gkritzalis, T., Harris, I., Hauck, J., Haverd, V., Hoppema, M., Klein Goldewijk, K., Jain, A. K., Kato, E., Körtzinger, A., Landschützer, P., Lefèvre, N., Lenton, A., Lienert, S., Lombardozzi, D., Melton, J. R., Metzl, N., Millero, F., Monteiro, P. M. S., Munro, D. R., Nabel, J. E. M. S., Nakaoka, S., O'Brien, K., Olsen, A., Omar, A. M., Ono, T., Pierrot, D., Poulter, B., Rödenbeck, C., Salisbury, J., Schuster, U., Schwinger, J., Séférian, R., Skjelvan, I., Stocker, B. D., Sutton, A. J., Takahashi, T., Tian, H., Tilbrook, B., Laan-Luijkx, I. T. van der, Werf, G. R. van der, Viovy, N., Walker, A. P., Wiltshire, A. J. and Zaehle, S.: Global Carbon Budget 2016, Earth Syst. Sci. Data, 8(2), 605–649, doi:10.5194/essd-8-605-2016, 2016.

Rödenbeck, C.: Estimating CO2 sources and sinks from atmospheric mixing ratio measurements using a global inversion of atmospheric transport, Max Planck Institute for Biogeochemistry., 2005.

Rödenbeck, C., Houweling, S., Gloor, M. and Heimann, M.: CO2 flux history 1982–2001 inferred from atmospheric data using a global inversion of atmospheric transport, Atmos Chem Phys, 3(6), 1919–1964, doi:10.5194/acp-3-1919-2003, 2003.

Stephens, B. B., Gurney, K. R., Tans, P. P., Sweeney, C., Peters, W., Bruhwiler, L., Ciais, P., Ramonet, M., Bousquet, P., Nakazawa, T., Aoki, S., Machida, T., Inoue, G., Vinnichenko, N., Lloyd, J., Jordan, A., Heimann, M., Shibistova, O., Langenfelds, R. L., Steele, L. P., Francey, R. J. and Denning, A. S.: Weak Northern and Strong Tropical Land Carbon Uptake from Vertical Profiles of Atmospheric CO2, Science, 316(5832), 1732–1735, doi:10.1126/science.1137004, 2007.

Wang, W., Ciais, P., Nemani, R. R., Canadell, J. G., Piao, S., Sitch, S., White, M. A., Hashimoto, H., Milesi, C. and Myneni, R. B.: Variations in atmospheric CO2 growth rates coupled with tropical temperature, Proc. Natl. Acad. Sci., 110(32), 13061–13066, doi:10.1073/pnas.1219683110, 2013.

Wang, X., Piao, S., Ciais, P., Friedlingstein, P., Myneni, R. B., Cox, P., Heimann, M., Miller, J., Peng, S., Wang, T., Yang, H. and Chen, A.: A two-fold increase of carbon cycle sensitivity to tropical temperature variations, Nature, 506(7487), 212–215, doi:10.1038/nature12915, 2014.

van der Werf, G. R., Randerson, J. T., Collatz, G. J., Giglio, L., Kasibhatla, P. S., Arellano, A. F., Olsen, S. C. and Kasischke, E. S.: Continental-Scale Partitioning of Fire Emissions During the 1997 to 2001 El Niño/La Niña Period, Science, 303(5654), 73–76, doi:10.1126/science.1090753, 2004.

Yin, Y., Ciais, P., Chevallier, F., van der Werf, G. R., Fanin, T., Broquet, G., Boesch, H., Cozic, A., Hauglustaine, D., Szopa, S. and Wang, Y.: Variability of fire carbon emissions in equatorial Asia and its nonlinear sensitivity to El Niño, Geophys. Res. Lett., 2016GL070971, doi:10.1002/2016GL070971, 2016.

Acknowledgements

We thank Taejin Park from Department of Earth and Environment, Boston University for making the NDVI data available. C.Y. and P.C. acknowledge funding from the European Commission's 7th Framework Programme, under grant agreement number 603542 (LUC4C). The work of F.C. was funded by the Copernicus Atmosphere Monitoring Service, implemented by the European Centre for Medium-Range Weather Forecasts (ECMWF) on behalf of the European Commission. We thank all the scientists involved in the surface and aircraft measurement of atmospheric CO_2 concentration and in archiving these data and making them available.

Author contributions

P.C., F.C., C.Y. and A.B. conceived the study. C.Y. performed the analysis and made the first draft. F.C. and C.R. provided the inversion data. All authors contributed to interpretation of the results and drafting the paper.

Figure 1 Year 2015 as the greenest year over the period 2000-2015. **(a)** Distribution of seasons for which 2015 NDVI ranks the highest during the period 2000-2015. Yellow-coloured pixels indicate grid cells where 2015 NDVI ranks highest for more than one season. For each season, the fraction of global vegetated land area for which 2015 NDVI ranks highest is shown in the inset colour bar. **(b)** Temporal evolution of the percentage of vegetated land with highest NDVI over 2000-2015 for each season and different years. The sum total of vertical-axis values for each season over all years is 100%. Q1 = January–March; Q2 = April–June; Q3 = July–August; Q4 = September–December.

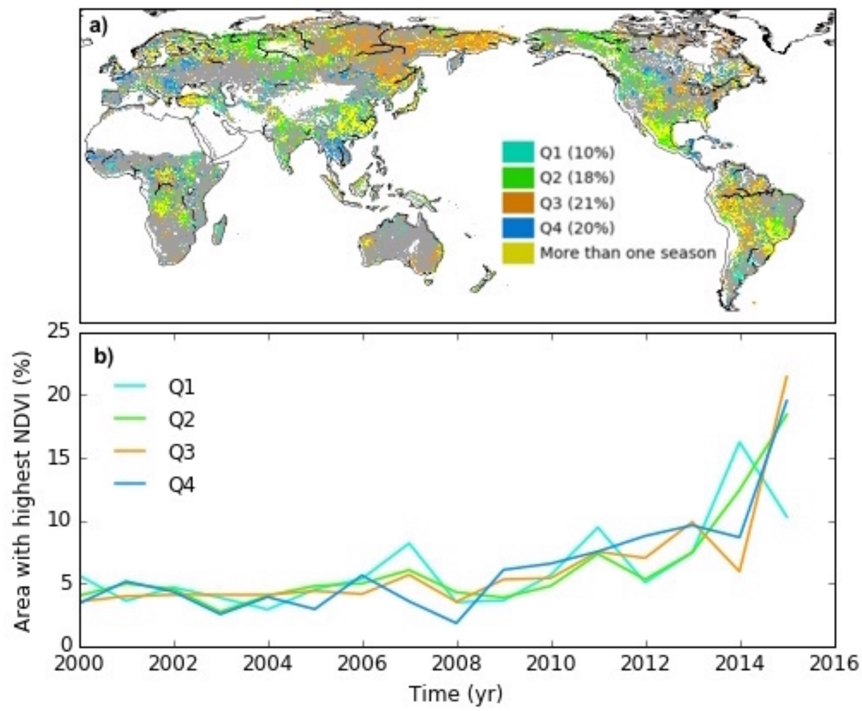

Atmos. Chem. Phys. Discuss., doi:10.5194/acp-2016-1167, 2017
Manuscript under review for journal Atmos. Chem. Phys.
Published: 12 January 2017

Figure 2 Global carbon fluxes and atmospheric CO_2 growth rates for 1981–2015. (a) Carbon emissions from fossil fuel and industry used in the CAMS (blue) and Jena04 (orange) inversions, **(b)** annual atmospheric CO_2 growth rate (AGR, in red) from NOAA/ESRL linked with Multivariate ENSO Index (in purple), and **(c)** land and **(d)** ocean carbon sinks for 1981-2015. Emissions and land and ocean carbon sinks from the Global Carbon Project (GCP, in black) are also shown for comparison. In subplots c and d, a carbon flux of 0.45 Pg C yr^{-1} was used to correct inversion-derived land and ocean sinks to account for pre-industrial land-to-ocean carbon flux as in Le Quéré et al. (2016). All numbers indicate values in 2015 (Pg C yr^{-1}), with those in brackets showing linearly detrended anomalies for the same year.

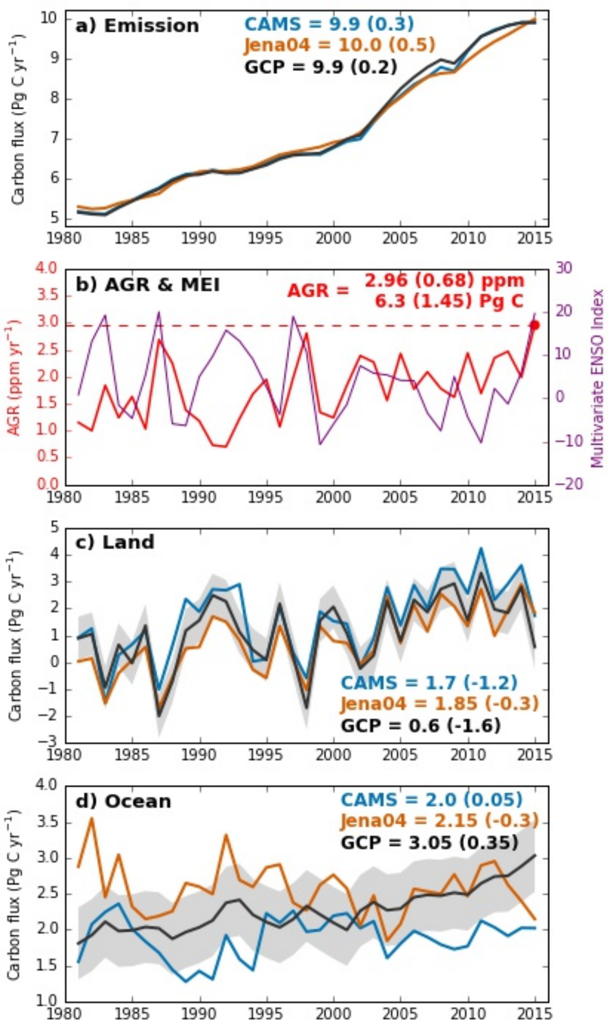

Figure 3 Seasonal land carbon uptake anomalies in 2015. Data are linearly detrended over 1981-2015 for different seasons in 2015, by CAMS (blue) and Jena04 (orange) inversion data. Open or solid dots indicate seasonal values (Pg C seasaon^{-1}) and vertical bars indicate annual sum (Pg C yr^{-1}). Data are shown for: **(a)** boreal and temperate Northern Hemisphere (BoTeNH, > 23.5°N), **(b)** tropics and southern extratropical hemisphere (TroSH, < 23.5°N) and **(c)** the whole globe. Solid dots indicate seasonal land carbon uptake anomalies below 10th or above 90th percentiles over 1981-2015.

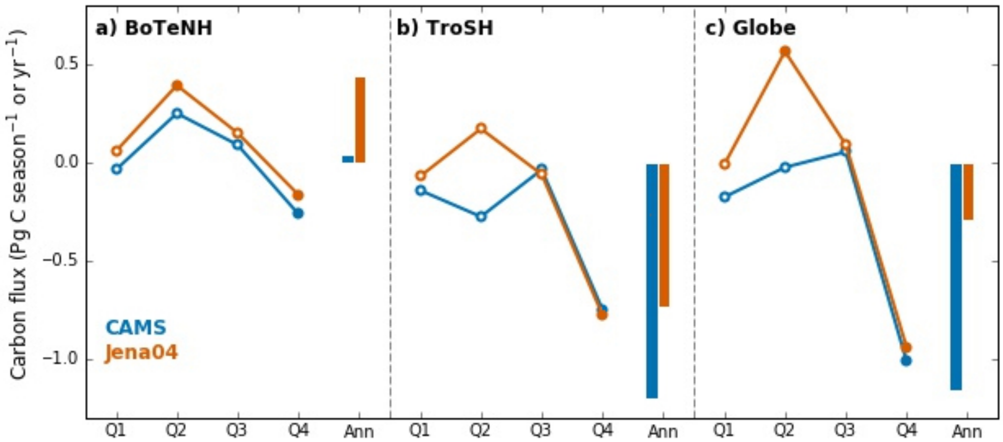

Atmos. Chem. Phys. Discuss., doi:10.5194/acp-2016-1167, 2017
Manuscript under review for journal Atmos. Chem. Phys.
Published: 12 January 2017

Atmospheric Chemistry and Physics Discussions

549 **Figure 4 Extremeness of transitions in seasonal land carbon uptake anomaly in 2015.** Histograms for seasonal land carbon uptake transitions over 1981-2015 for boreal and temperate Northern Hemisphere (BoTeNH, latitude > 23.5°N), tropics and extratropical Southern Hemisphere (TroSH, latitude < 23.5°N) and the whole globe. Transition between two consecutive seasons is defined as the linearly detrended land carbon uptake anomaly in a given season minus that in the former one. Coloured bars show histograms for CAMS data (red colour for a negative transition and green colour for a positive one), with the vertical-axis indicating frequency and blue solid vertical line indicating year 2015. Grey step lines indicate histograms for Jena04 data overlaid on top of CAMS data, with vertical orange solid lines indicating values for 2015.